Synthesis of ZnO semiconductor nanoparticles using extracts of *Capsicum annuum L.* for photocatalytic activity in degradation of polluting dyes

M. J. Rodríguez-Ortiz [a], E. Lugo-Medina [b, *], C. A. Soto-Robles [b], O. Nava [c], F. Aguilera Molina [a], Y. A. Báez-López [a], R. V. Quevedo-Robles [a], A. Carrillo-Castillo [d], F. Moreno-Osuna [b], R. Ranjithkumar [e], R. C. Villarreal Sánchez [a]

[a] *Faculty of Engineering, Architecture and Design, Autonomous University of Baja California, Ensenada, Baja California. C.P. 22860, México*

[b] *Tecnológico Nacional de México/IT de Los Mochis, Los Mochis, Sinaloa. C.P. 81259, México*

[c] *Centro de Nanociencias y Nanotecnología-UNAM, Ensenada, Baja California. C.P. 22800, México.*

[d] *Instituto de Ingeniería y Tecnología, Universidad Autónoma de Ciudad Juárez, Ciudad Juárez, C.P. 32310, Chihuahua, México*

[e] *Center for Global Health Research, Saveetha Medical College and Hospital, Saveetha Institute of Medical and Technical Sciences (SIMATS), Saveetha University, Chennai, 602105, Tamil Nadu, India*

In this work, ZnO semiconductor nanoparticles were green-synthesized using *Capsicum annuum L.* var. Caribe pepper extracts at 1%, 2%, and 4% w/v (weight/volume) as stabilizing agents. The nanoparticles were applied in photocatalytic processes for the degradation of Methylene Blue (MB), Methyl Orange (MO), and Rhodamine B (RhB) in aqueous media. Characterization involved Fourier Transform Infrared Spectroscopy (FT-IR), identifying the Zn-O bond at 421 cm^{-1}. X-Ray Diffraction (XRD) analysis revealed a hexagonal Wurtzite-type crystalline phase with crystallite sizes ranging from 13 to 23 nm. Scanning Electron Microscopy (SEM) showed hemispherical clusters smaller than 5 micrometers. UV–Visible spectrophotometry determined band gap values between 3.05 and 3.13 eV. These materials exhibited significant photocatalytic degradation efficiency for the tested dyes.

(Received August 2, 2024; Accepted January 15, 2025)

Keywords: Nanoparticle synthesis, ZnO, Polluting dyes, Photocatalysis, *Capsicum annuum L.*

1. Introduction

The quality of our environment has reached a critical level in the context of globalized human society, profoundly impacting the health of living organisms and the economic stability of nations worldwide. The issue of water pollution ranks among the most critical concerns facing our planet, the discharge of effluents from industries that consume high amounts of water in their processes generates a considerable volume of organic pollutants such as industrial dyes [1, 2]. If the dye-containing residual waters are not treated, the receiving bodies of water will increase their organic carbon content, which will disrupt the usual path of light and disturb the equilibrium of normal processes such as photosynthesis and respiration, to name a few [3]. Furthermore, the majority of industrial dyes are not biocompatible, causing human beings serious health issues like skin irritation, eye injuries, dyspnea, vomit, and mutagenic and carcinogenic effects, among others [4].

Since the emergence of environmental concerns, a substantial body of research has been devoted to addressing the proper treatment of water. Currently, the treatment procedures are usually classified into individual methods known as physical unit operations (e.g., filtration,

* Corresponding author: eder.lm@mochis.tecnm.mx
https://doi.org/10.15251/JOR.2025.211.47

sedimentation, etc.) [5], chemical unit operations (e.g., precipitation, adsorption, etc.) [6], and biological unit operations (e.g., biological aerated filtration, activated sludge, etc.) [7]. The use of conventional methods, be it physical, chemical, or biological, proves to be insufficient for the thorough elimination of pollutants and can generate still harmful sub-products; moreover, their set-up process could be troublesome and expensive [8].

Emerging technologies, such as heterogeneous photocatalysis, have gained traction. This method employs semiconductor oxides, acting as photocatalysts, under visible or UV light to initiate redox reactions that produce highly oxidative species like the hydroxyl radical (OH•) [9]. Unlike conventional methods, photocatalysis can transform organic pollutants into benign compounds without generating harmful by products. Some of the most active photocatalysts used nowadays are tin oxide (SnO_2) [10], titanium dioxide (TiO_2) [11], cadmium sulfide (CdS) [12], zirconium dioxide (ZrO_2) [13], tungsten oxide (WO_3) [14], cadmium telluride (CdTe) [15], and zinc oxide (ZnO) [16].

Presently, zinc oxide (ZnO) as a nanostructured photocatalyst has gained popularity and importance for the purpose of degradation of water pollutants [17], particularly ZnO nanoparticles due to their good physical and chemical properties that make it potentially good for the photocatalysis process [18], some remarkable characteristics are: it presents a Wurtzite like hexagonal structure at ambient conditions, it has a great band gap energy (3.37 eV) [19-20], a large surface area and consequently a high catalytic activity, good chemical and mechanical stability, among others [21].

There exist different methods for synthesizing nanoparticles: physical methods, which are generally costly and work with difficult to control variables (e.g., colloidal dispersion, vapor condensation, etc.) [22-23]; chemical methods, which usually use toxic compounds (e.g., pyrolysis, electrodeposition, etc.) [24-26], and biological methods. The last are still a new trend that emerged from nanotechnology and fundamentals of green chemistry and were driven by the environmental need to overcome the problems that conventional methods entail.

The green synthesis of nanoparticles is an environmentally respectful and profitable method [27], which takes benefit from chemical compounds found in natural sources such as microorganisms (bacteria, fungi, algae, etc.) and plants [28]. Plant extracts rich in compounds such as flavonoids, capsaicinoids, terpenoids, and phenolic acids act as reducing and stabilizing agents, facilitating nanoparticle synthesis without the use of toxic chemicals and yielding stable nanoparticles [29].

In this work, *Capsicum annuum L.* Caribe pepper was used as the natural source for synthesizing the nanoparticles. Its extract contains compounds of interest due to their chemical composition, such as flavonoids (e.g., lutein and quercetin), capsaicinoids (e.g., capsaicin), terpenoids, and phenolic acids (e.g., vanillic, gallic, and caffeic acid) [30, 31]. For this, it is a great candidate to be used. Characterization techniques included SEM/EDS, XRD, FTIR, photoluminescence (PL), and UV-Vis spectroscopy. The synthesized ZnO nanoparticles were evaluated for their photocatalytic activity using UV-Vis spectrophotometry, demonstrating their potential for degrading model dyes such as Methylene Blue (MB), Methyl Orange (MO), and Rhodamine B (RhB).

2. Experimental details

2.1. Materials

Fruit from *Capsicum annuum L.*, variety Caribe pepper locally bought in Baja California, Mexico was used. Zinc nitrate hexahydrate ($Zn(NO_3)_2•6H_2O$) sourced through Sigma Aldrich was used as Zinc precursor. The organic dyes to be tested for their photocatalytic degradation by the ZnO nanoparticles were bought from FagaLab: Methylene Blue (373.9 g/mol at 99% purity), Methyl Orange (327.34 g/mol at 95% purity), and Rhodamine B (479.01 g/mol at 95% purity). Deionized water was used as media throughout the experiment.

2.2. Extract preparation

The fruit pericarp of the *Capsicum annuum L.*, variety Caribe pepper was used to obtain the extract. First, it was dried for 6 h, then ground until it became a fine powder. Subsequently, the

powder was used for the preparation of suspensions at different concentrations of 0.5g, 1g, and 2g with 50 mL deionized water (1%, 2%, and 4% w/v (weight/volume), respectively). After stirring for 2 h at 25 °C, the various concentrations were placed in a sous-vide at 60 °C for another 2 h. The suspensions were then filtered through Whatman N° 4 filters and stored for its use during synthesis.

2.3. Synthesis of ZnO nanoparticles

Green ZnO nanoparticle synthesis was done by placing 2g of $Zn(NO_3)_2 \cdot 6H_2O$ in 42.5 mL of extract solutions that were previously prepared with different concentrations. The resulting solutions were stirred for 1 h and later introduced in a sous-vide at 60 °C for approximately 12 h until the consistency became pasty. Subsequent to calcination at 400 °C for 1 h, the samples were ground in an agate mortar. Following this, they were stored and labeled C1, C2, and C4 (In sequence: 1%, 2%, and 4%).

2.4. ZnO nanoparticles characterization

To understand the properties of the materials obtained using different extract concentrations in their synthesis, it is important to characterize them using various techniques to identify the effect of the extract on the formation of ZnO nanoparticles. The characterization techniques involved were: Fourier Transform Infrared Spectroscopy (FTIR): Using a Perkin Elmer Spectrum Two, in the range of 4000 cm^{-1} to 400 cm^{-1} with a resolution of 0.5 cm^{-1}, to identify the functional groups present. X-Ray Diffraction (XRD): Using a D2-Phaser Buker brand with a Cu K-α X-ray source (λ = 1.5406 Å) and an operating range of 2θ from 20° to 80°, to analyze the crystal structure and determine the crystallite sizes. Scanning Electron Microscopy and Energy Dispersive X-ray Spectroscopy (SEM/EDX): Using a JEOL JSM-6310LV to study the morphology and elemental composition of the sample. Ultraviolet-Visible Light Spectroscopy (UV-Vis): Using a Perkin Elmer Lambda 365 to determine the band gap values and dye degradation (photocatalytic activity). A sweep from 190 nm to 1000 nm is performed for the band gap study. Photoluminescence (PL) Studies: Using a FluoroMax-4 Horiba spectrometer with an excitation wavelength (λ_{exc}) of 320 nm.

2.5. Photocatalytic activity

Assessing the photocatalytic activity of the ZnO nanoparticles involved the preparation of separate solutions of dyes (MB, MO, and RhB) at 15 mg/L (15 ppm) of dye. 50 mg of the three different nanoparticles (C1, C2, and C4) were added to separate batches of 50 mL dye solutions. Subsequent to stirring the mixtures for 30 min without exposure to light, where they reach a chemical equilibrium of adsorption-desorption, the mixtures were exposed for 3 h to a UV lamp (a Polaris UV-1C Reactor, with a 10 W bulb and a dose of 18 mJ/cm2), and sunlight depending on the case study. Aliquots of 2 mL were taken. In the first hour, aliquots were taken every 10 min, after that time, aliquots were taken every 30 min up to 3 h. To carry out the concentration measurement, the aliquots were analyzed by UV-Vis, which monitored the characteristic absorption peaks of each dye: 664 nm-MB, 464 nm-MO and 553 nm-RhB.

The equation describing the degradation behavior is:

$$\%\ of\ photodegradation = \frac{C_0 - C_t}{C_0}\ x\ 100$$

where C_0 is initial dye concentration and C_t is dye concentration at a given time.

3. Results and discussions

3.1. Fourier transform infrared spectroscopy

The substituent chemical groups present in the fruit wall of *Capsicum annuum L.* var. Caribe peppers and in the ZnO nanoparticles are depicted in Fig. 1. The spectra of the three obtained ZnO nanoparticles are compared against that of pure extract. All of the nanoparticles

spectra denote a band in a range between 420 to 430 cm^{-1} associated with the bending vibration of the Zn-O bond (Fig. 1 B), as reported in the literature [32], which ratifies the formation of ZnO. On another hand, functional groups comprising the *Capsicum annuum L.* pericarp molecules are made evident through specific vibration signals: bands at 3295 and 2921 cm^{-1} (H–O–H and C-H) can be attributed to water and phenol groups; and others bands at 1733 (C=O), 1625 (C=C), 1403, and 1028 cm^{-1} (C-H) are associated to the bending and stretching of aromatic groups (Fig. 1 A). Similar signals are observed in the three biosynthesized samples (C1, C2, and C4), ratifying the presence of traces of phytochemicals derived from *Capsicum annuum L.*

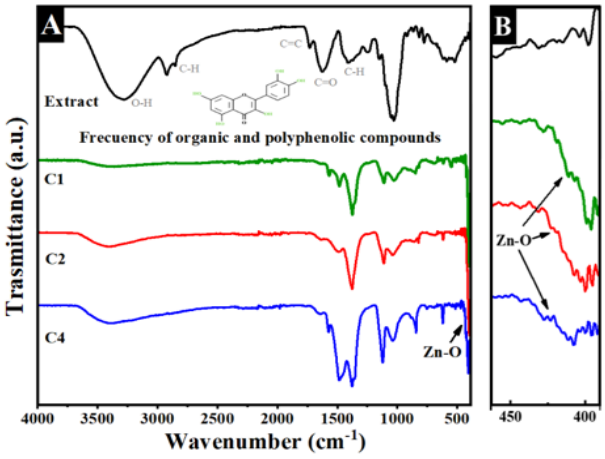

Fig. 1. FTIR Spectra of pure extract and obtained ZnO nanoparticles (A) and infrared region centered between 450 to 400 cm^{-1} (B).

3.2. Nanoparticle formation mechanism

The possible nanoparticle formation mechanism is shown in Fig. 2, which is explained on the basis that the biomolecules present in *Capsicum annuum L.* var. Caribe pepper pericarp (i.e. flavonoids, capsaicinoids, carotenoids, gallic acid, among others) extract act as stabilizing and reducing agents in the synthesis process. Which by hydrolysis, these aromatic hydroxyls compounds form complex bounds with the precursor salt ($Zn(NO_3)_2$) binding with zinc ions, this, in turn, begins a nucleation process which ends in nanoparticle formation during calcination as organic matter is removed [33, 34].

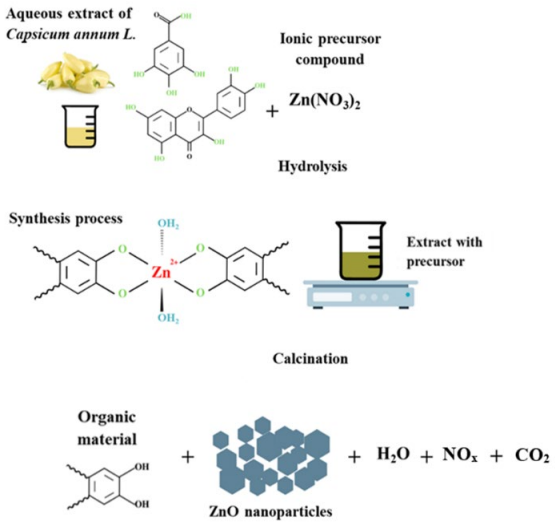

Fig. 2. Possible formation mechanism of ZnO nanoparticles synthesized with Capsicum annuum L. var. Caribe pepper extracts.

3.3. Photoluminescence spectroscopy

Fig. 3. shows the Photoluminescent (PL) spectra at room temperature of the ZnO nanoparticles synthesized with *Capsicum annuum L.* var. Caribe pepper. The spectra exhibit a broad emission from 390 to 600 nm wavelength, which is more intense as the extract concentration increases. The bands in the visible region are associated with electron-hole recombination at deep-level (DL) emission. This characteristic of ZnO NPs is attributed to the recombination of photogenerated electrons (e-), which is induced by defects and structural impurities comprising zinc and oxygen vacancies, and interstitial oxygen [35, 36]. Additionally, as seen Fig. 3, a small peak at around 390 nm (UV region) is seen, often linked to photogenerated hole (h+) recombination [37, 38].

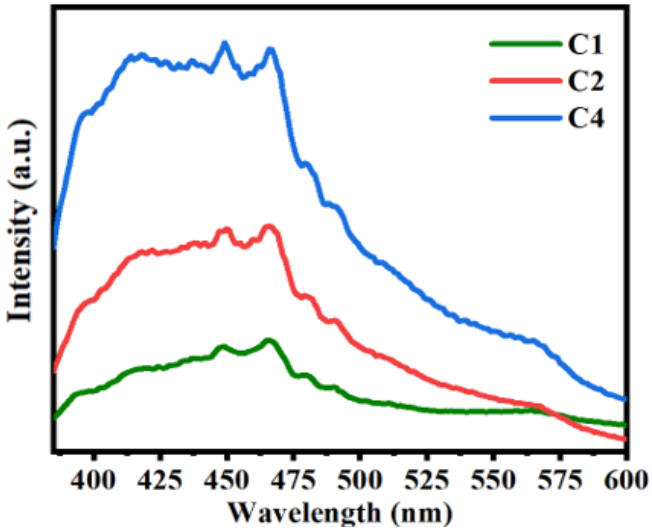

Fig. 3. PL spectra of ZnO nanoparticles.

3.4. Characterization of TiO_2 nanoparticles (Nps)

Fig. 4 presents the diffractograms of ZnO nanoparticles synthesized using *Capsicum annuum L.* var. Caribe pepper. These diffractograms are utilized to identify the crystalline phases of the ZnO nanoparticles. The XRD patterns depict different diffraction peak and intensities for the three different nanoparticles. The 36.28°, 31.80°, and 34.45° 2θ values, with their respective (101), (100), and (002) crystal planes, are the most prominent peaks for the Wurtzite-type, hexagonal crystalline phase, characteristic of ZnO nanoparticles (JCPDS: 36-1451) [39]. Lesser peaks at 47.57°, 56.62°, 62.88°, 67.93°; indexed to the planes (102), (110), (103), (112), respectively, are also associated with the Wurtzite crystalline phase. Additionally, other peaks are observed, which correspond to the KCl phase [40] due to the chemical composition of the Caribe peppers, which contain Potassium (K) [41].

Debye-Scherrer's formula was used to calculate crystallite size:

$$\tau = \frac{(K\,\lambda)}{(\beta\cos\theta)}$$

Here, τ is average crystallite size, K is a dimensionless constant approximately equal to 0.9, λ is X-ray wavelength, β is Full Width at Half Maximum (FWHM), and θ is Bragg's angle [42].

Average crystallite sizes calculated from the X-Ray diffractograms were 23.35 for C1, 14.71 for C2, and 13.99 nm for C4. It can be noted that the lower the extract concentration used for synthesizing the ZnO nanoparticles, the more defined and narrow the diffraction peaks are, which indicates that the amount of extract used influenced crystallinity and crystalline size.

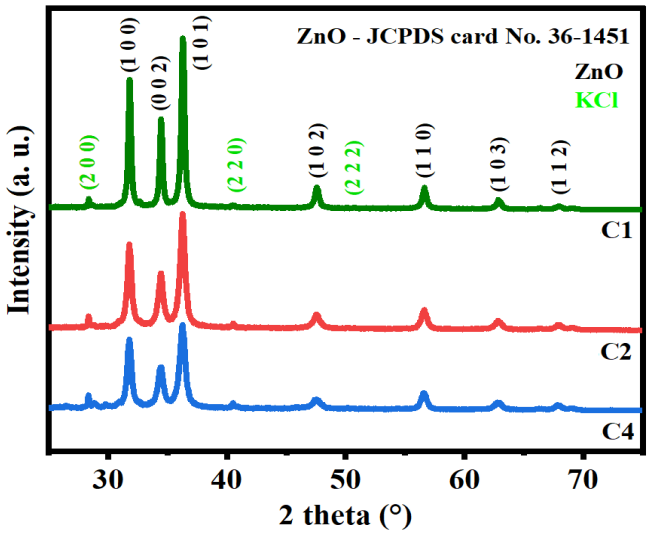

Fig. 4. XRD diffractograms of ZnO nanoparticles.

3.5. Surface morphology and elemental analysis

Scanning electron micrographs and elemental composition of the ZnO nanoparticles synthesized with *Capsicum annuum L.*, var. Caribe pepper is displayed in Fig 5. In the micrographs of samples C1, C2, and C4 (Fig. 5 A, B, and C, respectively), clusters with irregular, hemispherical shapes, and sizes smaller than 5 micrometers were observed. A trend was noted in relation to extract concentration: lower concentrations resulted in larger cluster sizes, and vice versa.

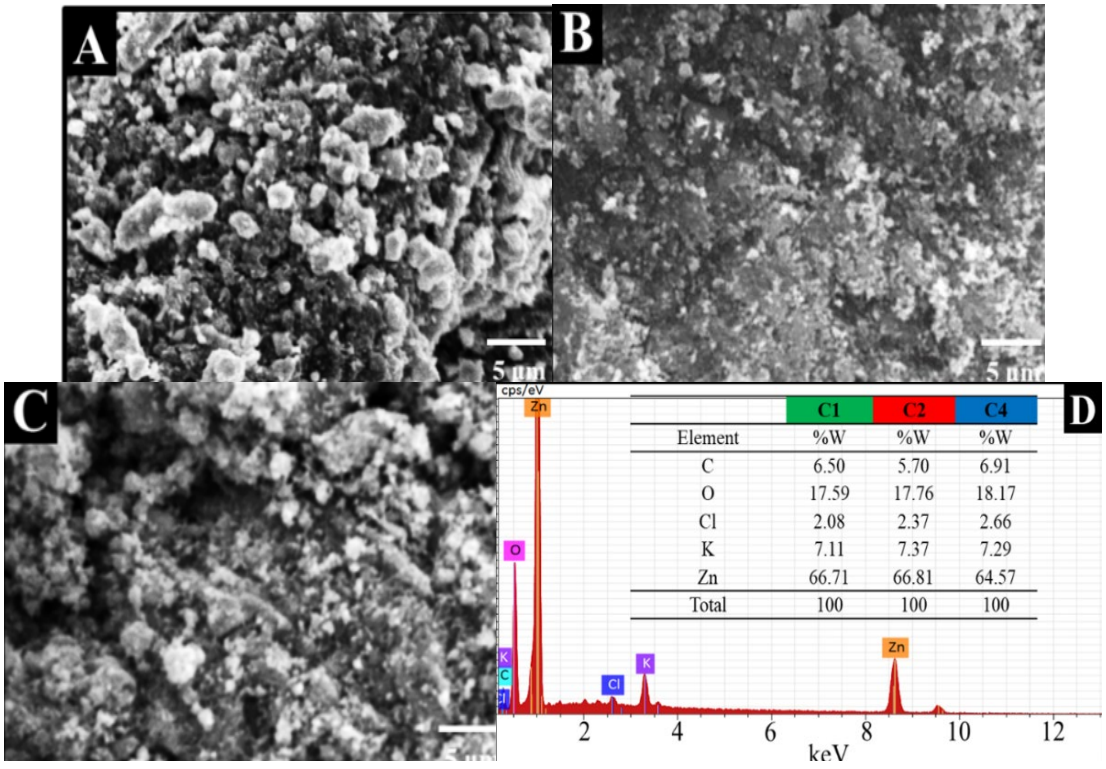

Element	C1 %W	C2 %W	C4 %W
C	6.50	5.70	6.91
O	17.59	17.76	18.17
Cl	2.08	2.37	2.66
K	7.11	7.37	7.29
Zn	66.71	66.81	64.57
Total	100	100	100

Fig. 5. SEM micrographs for C1 (A), C2 (B), and C4 (C) nanoparticles are shown with a 5 µm scale and the study of elemental composition (D), respectively.

In addition, the samples were subjected to elemental composition analysis where the weight percentage (W%) of each element present was obtained. The three samples (C1, C2, and C4) exhibited similar elemental composition of Zn, O, C, Cl, and K with a variation in the weight percentage of the elements. It can be noted that with a higher concentration of the extract, there is a slight increase in elements different than those from ZnO (K and Cl), which is attributed to *Capsicum annuum L.* var. Caribe pepper extract composition.

3.6. Optical properties

UV-Vis absorbance spectra were analyzed for the band gap calculation of the ZnO nanoparticles. Fig. 6 A displays the absorption spectra of the ZnO samples, where an absorbance signal is observed in the range between 300 and 400 nm, with absorbance bands at 372 nm, 369 nm and 365 nm, respectively.

Band gap energies of the samples were calculated through the TAUC model:

$$\alpha\,(\mathrm{v})\mathrm{hv} = \mathrm{K}(\mathrm{hv} - \mathrm{E}g)\text{^}\mathrm{n}$$

Here Eg is band gap energy, hv is energy of incident photon, K is a constant, and α(v) is the Beer-Lambert Law absorption coefficient [43]. The type of transition modifies exponent n; for ZnO nanoparticles, its value is ½ since it is a permitted direct transition. The band gap energy values obtained were 3.05, 3.11, and 3.13 eV for C1, C2, and C4 (Fig. 6 B, C and D,), respectively. These results closely resemble findings re-ported elsewhere for ZnO nanoparticles [44]. Furthermore, it can also be observed that an increase in extract percentage for ZnO nanoparticles synthesis raised the band gap value.

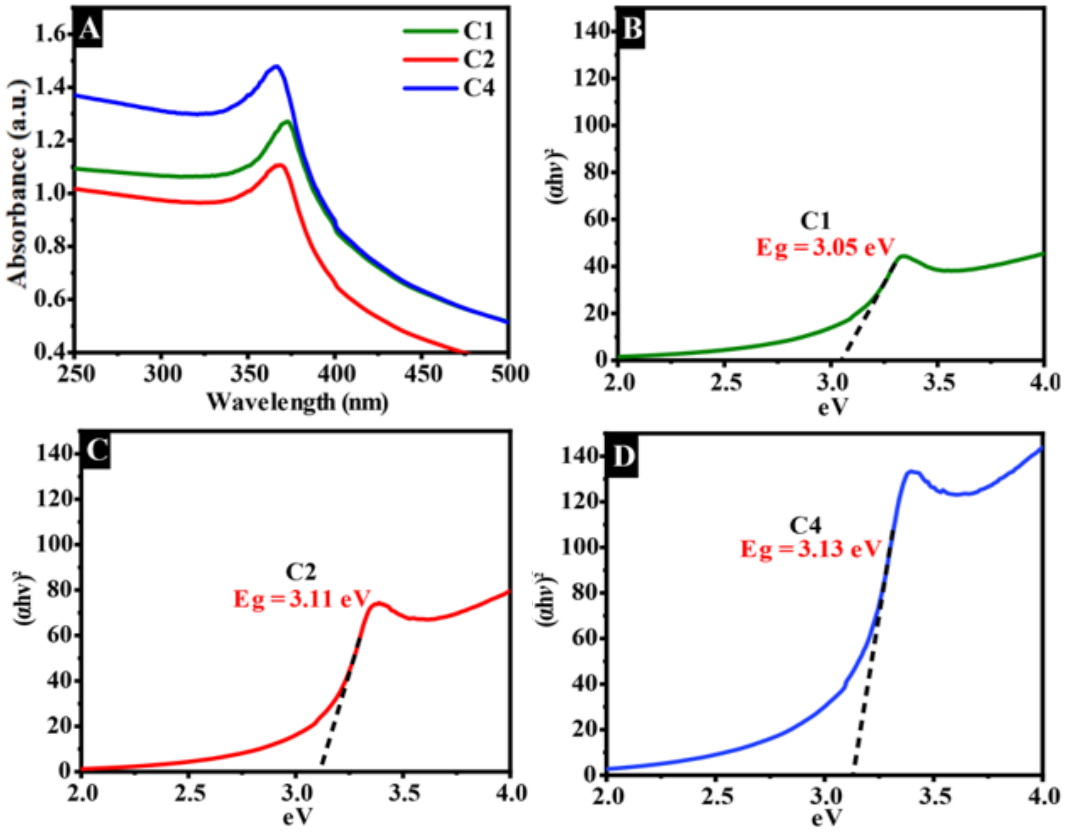

Fig. 6. ZnO nanoparticle absorption spectra (A) and band gap values (B, C, and D).

3.7. Photocatalytic activity

The photocatalytic activity evaluations of the ZnO nanoparticles through MB degradation under UV and sunlight irradiation are shown in Fig. 7. Shown in Fig. 7 A is the UV-Vis absorption spectra of the characteristic MB signal at 664 nm [45]. In the results under UV radiation of photocatalytic degradation of MB after 60 min of irradiation were 58.89%, 97.36% and 96.20% for the photocatalysts C1, C2, and C4, respectively (Fig. 7 B). In the results for the study under solar light irradiation, the photocatalysts after 60 minutes degraded 97.54%, 99.54% and 98.57% for C1, C2, and C4, respectively (Fig. 7 C). These findings reveal that the C2 sample yielded the best results compared to the other samples in both case studies (UV and sunlight irradiation).

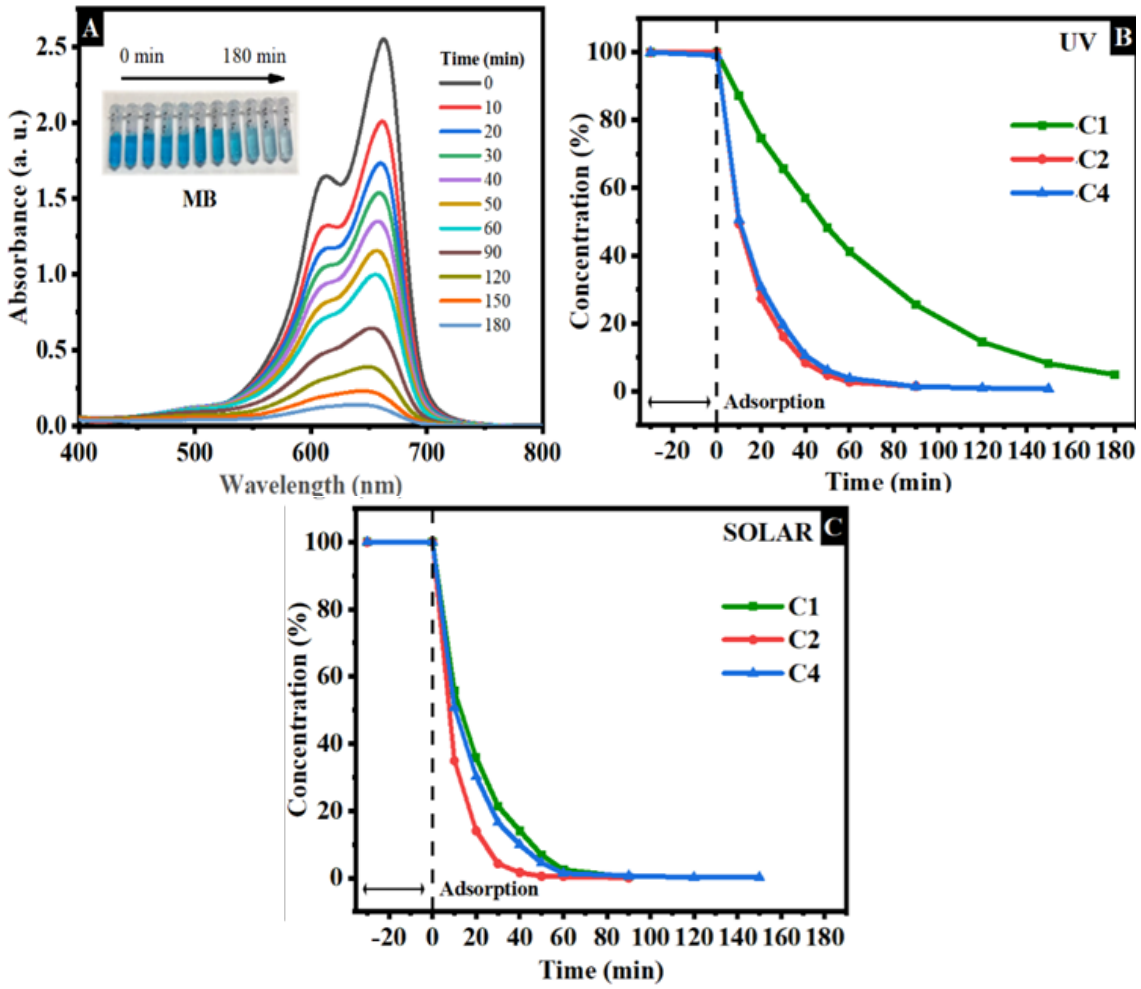

Fig. 7. MB UV-Vis absorption spectra (A). Photocatalytic degradation of MB using ZnO nanoparticles in solar (B) and UV (C) irradiation.

The photocatalytic activity evaluations of the ZnO nanoparticles through MO degradation under UV and sunlight irradiation are shown in Fig. 8. Shown in Fig. 8 A is the UV-Vis absorption spectra of the characteristic MO signal at 464 nm [46]. In the results under UV radiation of photocatalytic degradation of MO in 180 min of irradiation were 93.74%, 99.29% and 76.26% for the photocatalysts C1, C2, and C4, respectively (Fig. 8 B). In the results for the study under solar light irradiation, the same behavior was displayed but with a lower degradation after 180 min, with 57.94%, 85.82% and 59.48% of photocatalytic degradation for C1, C2, and C4, respectively (Fig. 8 C). In the case of this dye, the C2 sample was the best performer compared to the other samples.

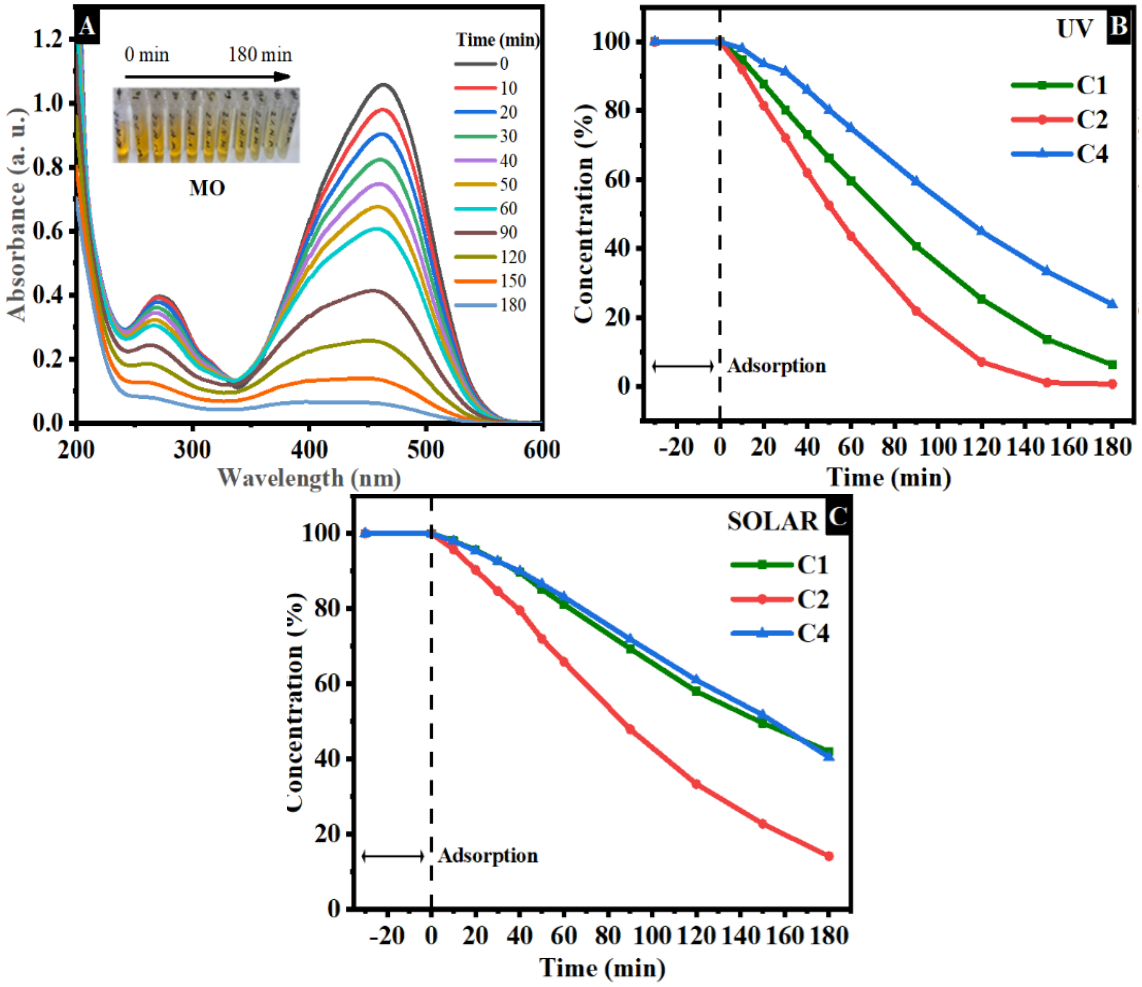

Fig. 8. MO UV-Vis absorption spectra (A). Photocatalytic degradation of MO using ZnO nanoparticles in solar (B) and UV (C) irradiation.

The photocatalytic activity evaluations of the ZnO nanoparticles through RhB degradation under UV and solar irradiation are shown in Fig. 9. Shown in Fig. 9 A is the UV-Vis absorption spectra of the characteristic RhB signal at 554 nm [47]. In the results under UV radiation of photocatalytic degradation of RhB in 180 min of irradiation were 54.38%, 85.86% and 56.83% for the photocatalysts C1, C2, and C4, respectively (Fig. 9 B). Whereas in the case study under sunlight irradiation, photocatalytic degradation percentages of 56, 54, and 69 were obtained for the samples C1, C2, and C4, respectively (Fig. 9 C). The C2 sample showed a better degradation percentage compared to the other samples under the two irradiations.

Table 1 presents a comparison of degradation results, indicating that the degradation percentages are comparable to or exceed those reported in the literature. This suggests that the synthesized ZnO nanoparticles are effective for use in the degradation of water pollutants, such as dyes.

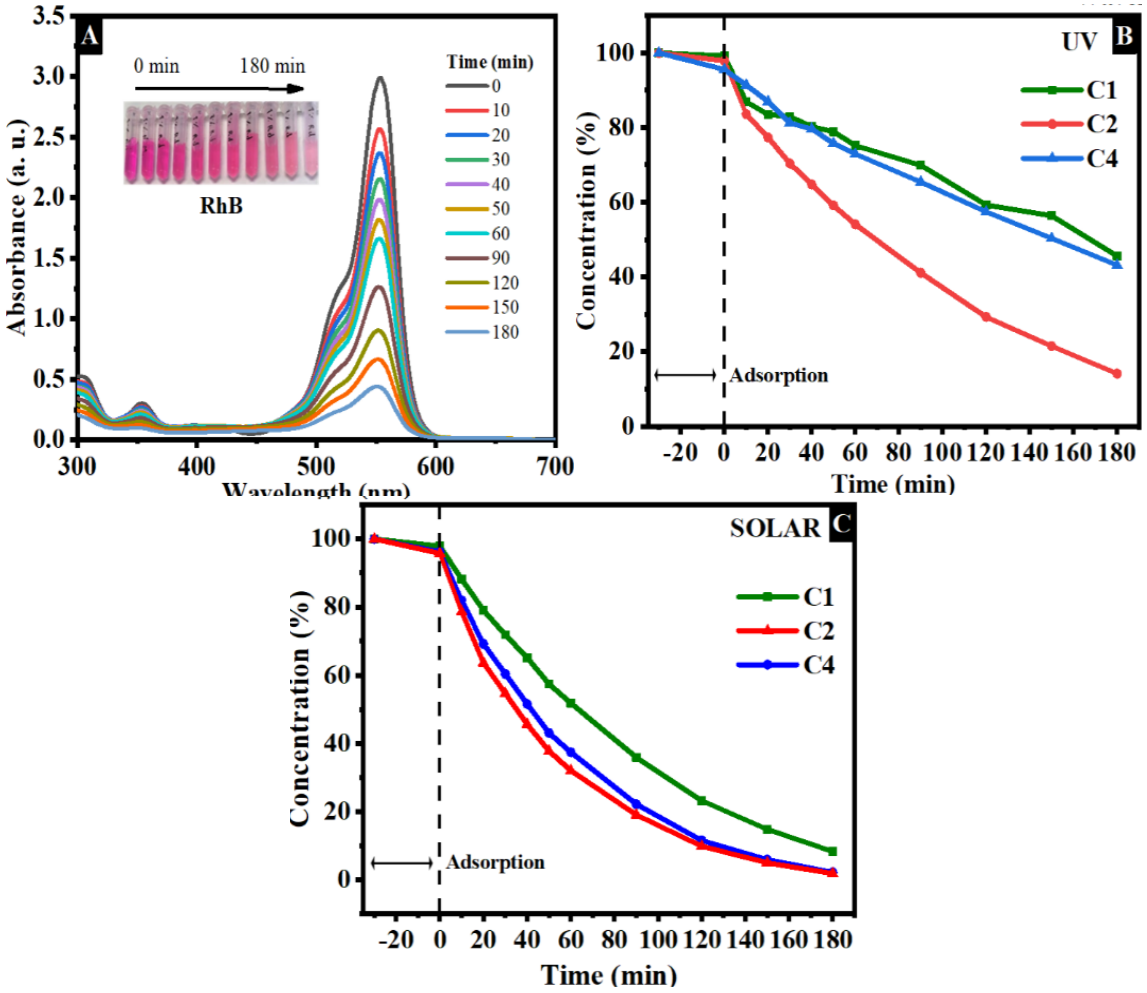

Fig. 9. RhB UV-Vis absorption spectra (A). Photocatalytic degradation of MO using ZnO nanoparticles in solar (B) and UV (C) irradiation.

Table 1. Comparation of degradation efficiency of ZnO nanoparticles

Extract (plant)	Time (min)	Degradation (%)	Pollutant	Year/Reference
Capsicum annuum L.	90	100	MB	This work
Capsicum annuum L.	120	93	MO	This work
Capsicum annuum L.	120	71	RhB	This work
Calotropis gigantea	120	50.4	RhB	2020 [52]
Scutellariabaicalensis	210	98.6	MB	2019 [53]
Citrus × paradisi	180	77	MB	2017 [54]
Calotropis procera	100	81	MO	2017 [55]
Eriobotrya japonica	200	57	MB	2020 [56]
Ziziphus jujuba	300	73	MB	2020 [57]
L. speciosa	120	93	MO	2017]

3.8. Degradation rate comparison

A kinetic study was performed to elucidate the degradation rates of the synthesized ZnO samples (C1, C2, and C4). A pseudo-first-order model was implemented through equation:

$$\mathrm{kt} = ln\frac{C_t}{C_0}$$

Here, C_0 is dye concentration at t=0 min; C_t is the concentration at any given time; k is pseudo-first-order rate constant [48, 49].

The calculated values are presented in Table 2. The samples showed similar degradation behaviors for the three dyes under both UV and sunlight irradiation, where C2 exhibited the highest photocatalytic activity with all dyes and both cases of radiation studied. This study confirms that ZnO nanoparticles synthesized with *Capsicum annuum L.,* variety Caribe pepper extract degrade polluting dyes (MB, MO, and RhB) in aqueous medium and these results are significant compared to other similar studies as shown in Table 2.

Table 2. Degradation constants of ZnO nanoparticles used dyes in UV and solar irradiation.

Sample	k (min^{-1})					
	MB		MO		RhB	
	Sol	UV	Sol	UV	Sol	UV
C1	0.06301	0.01697	0.00499	0.01484	0.01342	0.00375
C2	0.07744	0.04936	0.01082	0.02919	0.02108	0.01031
C4	0.04274	0.03389	0.00493	0.0076	0.02027	0.00436

3.9. Degradation mechanism

The schematic in Fig.10 describes the photocatalytic dye degradation mechanism by the ZnO nanoparticles synthesized using *Capsicum annuum L.*, var. Caribe pepper as natural source. The first stage of photocatalytic degradation is dye adsorption onto the nanoparticle surface. Next, depending on the case study, the reaction solutions are irradiated with solar or UV light, whose energies are greater than those of ZnO nanoparticles (hv ≥ Eg) and cause electrons (e-) to be excited, moving to the conduction band resulting in the formation of holes (h+) in the valence band. The electrons and photogenerated holes on the surface react with O_2 and H_2O, leading to the formation of radicals with high oxidative power, such as superoxide (O_2^-) and hydroxyl (OH•) that degrade dyes down to the final H_2O and CO_2 molecules and other non-polluting sub-products [50, 51].

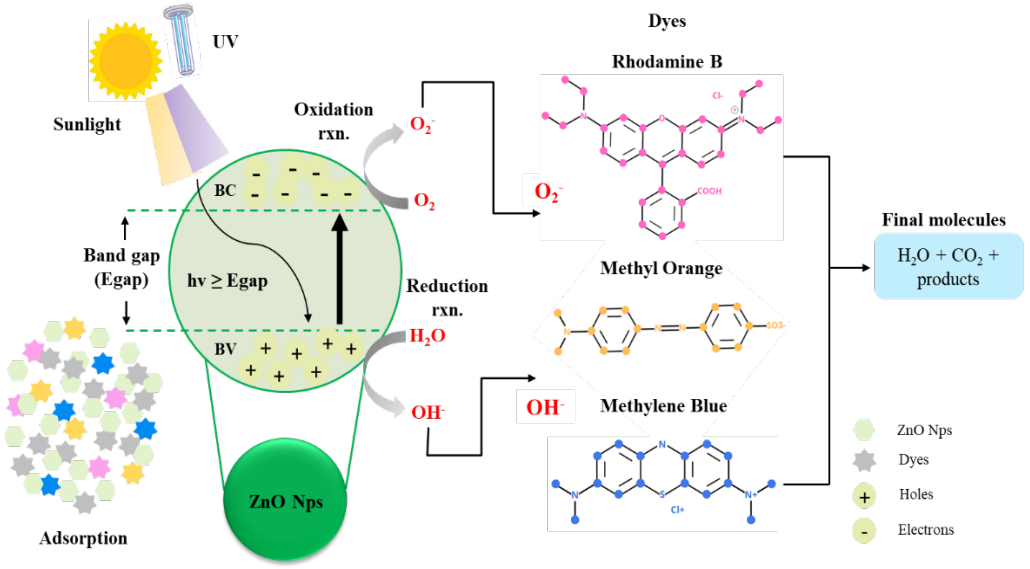

Fig. 10. Reaction mechanism for photocatalytic degradation of organic pollutants (MB, MO, and RhB) in aqueous systems by ZnO nanoparticles.

4. Conclusions

ZnO nanoparticles were produced by green synthesis using extracts obtained from the fruit pericarp of *Capsicum annuum L.,* variety Caribe pepper, and avoiding the use of toxic substances. The ZnO nanoparticles exhibited crystallite sizes from 13 to 23 nm with a Wurtzite-type crystalline phase, hemispherical clusters of sizes less than 5 micrometers were observed. Zn, O, Cl and K were identified as part of the elemental composition, and band gap energies were calculated within the 3.11 and 3.05 eV range. Complementarily, the application of the ZnO nanoparticles in the photocatalytic deg-radation of MB, MO, and RhB dyes was very good.

Sample C2 manifested the best photocatalytic activity, degrading 100% of MB after 90 min (UV) and 100% in 50 min (Sun); 99% (UV) and 85% (Sun) of MO in 180 min; and, 85% (UV) and 98% (Sun) of RhB in 180 min. Highlighting the fact that the behavior of the 4%-extract sample (C4) was similar to that of the 2% sample (C2), which confirmed that medium and high concentrations of extract withdrawn from Caribe pepper affected physical and chem-ical properties of the ZnO nanoparticles resulting in a positive outcome for its application towards water treatment through photocatalysis.

Acknowledgements

The authors thank the projects of the Autonomous University of Baja California (UABC) 402/3391 and 402/3751, as well as 402/1/C/58/24. This research was funded by the Frontera Science Project with number CF-2023-I-1805 of CONAHCyT.

References

[1] T. Sathish, N. Ahalya, M. Thirunavukkarasu, T.S. Senthil, Z. Hussain, M.I. Haque Siddiqui, H. Panchal, K. Sadasivuni, Alex. Eng. J. 86, 373 (2024); https://doi.org/10.1016/j.aej.2023.10.038

[2] P. Babuji, S. Thirumalaisamy, K. Duraisamy, G. Periyasamy, Water 15, 2532 (2023); https://doi.org/10.3390/w15142532

[3] T. Islam, M.R. Repon, T. Islam, Z. Sarwar, M.M. Rahman, Environ. Sci. Pollut. Res. 30, 9207 (2023); https://doi.org/10.1007/s11356-022-24398-3

[4] S. Dutta, S. Adhikary, S. Bhattacharya, D. Roy, S. Chatterjee, A. Chakraborty, D. Banerjee, A. Ganguly, S. Nanda, P. Rajak, J. Environ. Manage. 353, 120103 (2024); https://doi.org/10.1016/j.jenvman.2024.120103

[5] B. Azimi, S. Sepahvand, S. Ismaeilimoghadam, H. Kargarzadeh, A. Ashori, M. Jonoobi, S. Danti, J. Polym. Environ. 32, 345 (2023); https://doi.org/10.1007/s10924-023-02989-6

[6] M. Grzegorzek, K. Wartalska, B. Kaźmierczak, Int. Commun. Heat Mass Transf. 143, 106674 (2023); https://doi.org/10.1016/j.icheatmasstransfer.2023.106674

[7] A.I. Osman, E.M.A. El-Monaem, A.M. Elgarahy, C.O. Aniagor, M. Hosny, M. Farghali, E. Rashad, M.I. Ejimofor, E.A. López-Maldonado, I. Ihara, et al., Environ. Chem. Lett. 21, 2337 (2023); https://doi.org/10.1007/s10311-023-01603-4

[8] M.A. Hossen, A. Abd Aziz, N.Y. Yahya, K.H. Leong, L.C. Sim, M.U. Monir, K.D. Zoh, J. Environ. Chem. Eng. 11, 109610 (2023); https://doi.org/10.1016/j.jece.2023.109610

[9] S. Khan, T. Noor, N. Iqbal, L. Yaqoob, ACS Omega 9, 21751 (2024); https://doi.org/10.1021/acsomega.4c00887

[10] M.F.Lanjwani, M. Tuzen, M.Y. Khuhawar, Chem. Pap. 78, 4813 (2024); https://doi.org/10.1007/s11696-024-03431-4

[11] P. Akhter, F. Ali, A. Ali, M. Hussain, Diam. Relat. Mater. 141, 110702 (2024); https://doi.org/10.1016/j.diamond.2023.110702

[12] N. Mehrabanpour, A. Nezamzadeh-Ejhieh, S. Ghattavi, A. Ershadi, Appl. Surf. Sci. 614,

156252 (2023); https://doi.org/10.1016/j.apsusc.2022.156252

[13] W. Ahmed, J. Iqbal, Ceram. Int. 46, 25833 (2020); https://doi.org/10.1016/j.ceramint.2020.07.065

[14] S. Yuju, T. Xiujuan, S. Dongsheng, Z. Zhiruo, W. Meizhen, Ecotoxicol. Environ. Saf. 259, 11498 (2023); https://doi.org/10.1016/j.ecoenv.2023.114988

[15] S. Islam, A. Alshoaibi, H. Bakhtiar, K. Alamer, J. Mazher, Z.H. Alhashem, M.R. Hatshan, S.H. Aleithan, Mater. Res. Bull. 161, 112172 (2023); https://doi.org/10.1016/j.materresbull.2023.112172

[16] S. Ali, T. Sidra; T. Asghar, M.I. Jan, M. Waqas, T. Ali, R. Ullah, A. Bari, Catalysts 14, 337 (2024); https://doi.org/10.3390/catal14060337

[17] N.E. Zikalala, S. Azizi, S.A. Zikalala, I. Kamika, M. Maaza, A.A. Zinatizadeh, T. Mokrani, K. Kaviyarasu, Catalysts 12, 1442 (2022); https://doi.org/10.3390/catal12111442

[18] C.A. Aggelopoulos, O. Dolinski, Chemosphere 347, 140667 (2024); https://doi.org/10.1016/j.chemosphere.2023.140667

[19] A.M. El-Khawaga, M.A. Elsayed, M. Gobara, A.A. Suliman, A.H. Hashem, A.A. Zaher, M. Mohsen, S.S. Salem, Biomass Conv. Bioref. (2023).

[20] S.M. Mahdi Ismail, S.M. Ahmed, A.F. Abdulrahman, M.A. AlMessiere, J. Mol. Struct. 1280, 135063 (2023); https://doi.org/10.1016/j.molstruc.2023.135063

[21] K. Singh, H. Nancy, H. Kaur, P.K. Sharma, G. Singh, J. Singh, Chemosphere 313, 137322 (2023); https://doi.org/10.1016/j.chemosphere.2022.137322

[22] M. Saraswat, R.J. Sengwa, J. Mol. Liq. 385, 122350 (2023); https://doi.org/10.1016/j.molliq.2023.122350

[23] A.N.D. Krupa, R. Vimala, Mater. Sci. Eng. C. 61, 728 (2016); https://doi.org/10.1016/j.msec.2016.01.013

[24] Y.N. Hendri, Y. Rati, A.K.E. Auni, R. Marlina, R.; Munir, M.M.; Patah, A.; Darma, Y. Mater. Today Commun. 37, 107011 (2023); https://doi.org/10.1016/j.mtcomm.2023.107011

[25] S. Mitra, P. Patra, S. Pradhan, N. Debnath, K.K. Dey, S. Sarkar, Goswami, J. Colloid Interf. Sci. 444, 97 (2015); https://doi.org/10.1016/j.jcis.2014.12.041

[26] H.J. Biswal, P.R. Vundavilli, K. Mondal, N.P. Shetti, A. Gupta, Mater. Sci. Energy Technol. 6, 237 (2023); https://doi.org/10.1016/j.mset.2023.01.001

[27] S. Sasi, P.H. Fathima Fasna, T.K. Bindu Sharmila, C.S. Julie Chandra, J.V. Antony, V. Raman, A.B. Nair, H.N. Ramanathan, J. Alloys Compd. 924, 166431 (2022); https://doi.org/10.1016/j.jallcom.2022.166431

[28] K. Singh, Nancy, G. Singh, Environ. Res. 219, 114952 (2023); https://doi.org/10.1016/j.envres.2022.114952

[29] V. Dhiman, N. Kondal, Prashant Environ. Res. 216, 114751 (2023); https://doi.org/10.1016/j.envres.2022.114751

[30] A.S. Antonio, L.S.M. Wiedemann, V.F.V. Junior, RSC Adv. 8, 25767 (2018); https://doi.org/10.1039/C8RA02067A

[31] L.Á. Medina-Juárez, D.M.A. Molina-Quijada, C.L.D.T. Sánchez, G.A. González-Aguilar, N. Gámez-Meza, Interciencia 37, 588 (2012).

[32] L. Umaralikhan, M. Jaffar, J. Mater. Sci. Mater. Electron. 28, 7677 (2017); https://doi.org/10.1007/s10854-017-6461-1

[33] T. Karnan, S.A.S. Selvakumar, J. Mol. Struct. 1125, 358 (2016); https://doi.org/10.1016/j.molstruc.2016.07.029

[34] R. Chokkareddy, G.G. Redhi, Green Met. Nanoparticles Synth. Charact. Their Appl. Kanchi, S., Ahmed, S., Eds. 1, 113 (2018); https://doi.org/10.1002/9781119418900.ch4

[35] S.S. Mydeen, R.R. Kumar, M. Kottaisamy, V.S. Vasantha, J. Saudi Chem. Soc. 24, 393 (2020); https://doi.org/10.1016/j.jscs.2020.03.003

[36] M. Anbuvannan, M. Ramesh, G. Viruthagiri, N. Shanmugam, N. Kannadasan, Spectrochim.

Acta Part A Mol. Biomol. Spectrosc. 143, 304 (2015); https://doi.org/10.1016/j.saa.2015.01.124
[37] L. Fu, Z. Fu, Ceram. Int. 41, 2492 (2015); https://doi.org/10.1016/j.ceramint.2014.10.069
[38] R. Bekkari, D. Boyer, R. Mahiou, B. Jaber, Mater. Sci. Semicond. Process. 71, 181 (2017); https://doi.org/10.1016/j.mssp.2017.07.027
[39] K. Steffy, G. Shanthi, A.S. Maroky, S. Selvakumar, J. Adv. Res. 9, 69 (2018); https://doi.org/10.1016/j.jare.2017.11.001
[40] P.A. Luque, O. Nava, C.A. Soto-Robles, A.S. Vilchis-Nestor, H.E. Garrafa-Galvez, A. Castro-Beltran, J. Mater. Sci. Mater. Electron. 29, 17638 (2018); https://doi.org/10.1007/s10854-018-9867-5
[41] Y.M. Valadez Sánchez, E. Olivares Sáenz, R.E. Vázquez Alvarado, J.R. Esparza-Rivera, P. Preciado-Rangel, R.D. Valdez-Cepeda, J.L. García-Hernandez, Phyt. 85, 21 (2016); https://doi.org/10.32604/phyton.2016.85.021
[42] X. Zhang, Y. Chen, S. Zhang, C. Qiu, Sep. Purif. Technol. 172, 236 (2017); https://doi.org/10.1016/j.seppur.2016.08.016
[43] J. Tauc, R. Grigorovici, A. Vancu, Phys. status solidi. 15, 627 (1966); https://doi.org/10.1002/pssb.19660150224
[44] C.A. Soto-Robles, P.A. Luque, C.M. Gómez-Gutiérrez, O. Nava, A.R. Vilchis-Nestor, E. Lugo-Medina, A. Castro-Beltrán, Results Phys. 15, 102807 (2019); https://doi.org/10.1016/j.rinp.2019.102807
[45] S. Pal, S. Mondal, J. Maity, R. Mukherjee, Int. J. Nanosci. Nanotechnol. 14, 111 (2018).
[46] V.Q. Hieu, T.K. Phung, T.Q. Nguyen, A. Khan, V.D. Doan, V.A. Tran, Chemosphere 276, 130154 (2021); https://doi.org/10.1016/j.chemosphere.2021.130154
[47] E.S. Mehr, M. Sorbiun, A. Ramazani, S.T. Fardood, J. Mater. Sci. Mater. Electron. 29, 1333 (2018); https://doi.org/10.1007/s10854-017-8039-3
[48] F.Q. Ma, J.W. Yao, Y.F. Zhang, Y. Wei, RSC Adv. 7, 36288 (2017); https://doi.org/10.1039/C7RA06261C
[49] K. Durairaj, P. Senthilkumar, P. Velmurugan, K. Dhamodaran, K. Kadirvelu, S. Kumaran, J. Sol-Gel Sci. Technol. 90, 653 (2019); https://doi.org/10.1007/s10971-019-04922-7
[50] S.A. Younis, K.H. Kim, Catalysts 10, 1109 (2020); https://doi.org/10.3390/catal10101109
[51] V.O. Shikuku, W.N. Nyairo, Impact of textile dyes on public health and the environment, IGI Global. 205 (2020); https://doi.org/10.4018/978-1-7998-0311-9.ch010
[52] M. Saeed, M. Siddique, M. Ibrahim, N. Akram, M. Usman, M.A. Aleem, A. Baig, Environ. Prog. Sustain. Energy 39, e13408 (2020); https://doi.org/10.1002/ep.13408
[53] L. Chen, I. Batjikh, J. Hurh, Y. Han, Y. Huo, H. Ali, D.C. Yang, Optik (Stuttg) 184, 324 (2019); https://doi.org/10.1016/j.ijleo.2019.03.051
[54] O.J. Nava, C.A. Soto-Robles, C.M. Gómez-Gutiérrez, A.R. Vilchis-Nestor, A. Castro-Beltrán, A. Olivas, P.A. Luque, J. Mol. Struct. 1147, 1 (2017); https://doi.org/10.1016/j.molstruc.2017.06.078
[55] V.V. Gawade, N.L. Gavade, H.M. Shinde, S.B. Babar, A.N. Kadam, K.M. Garadkar, J. Mater. Sci. Mater. Electron. 28, 14033 (2017); https://doi.org/10.1007/s10854-017-7254-2
[56] M. Shabaani, S. Rahaiee, M. Zare, S.M. Jafari, LWT. 134, 110133 (2020); https://doi.org/10.1016/j.lwt.2020.110133
[57] M. Golmohammadi, M. Honarmand, S. Ghanbari, Spectrochim. Acta Part A Mol. Biomol. Spectrosc. 229, 117961 (2020); https://doi.org/10.1016/j.saa.2019.117961
[58] V.S. Saraswathi, J. Tatsugi, P.K. Shin, K. Santhakumar, J. Photochem. Photobiol. B Biol. 167, 89 (2017); https://doi.org/10.1016/j.jphotobiol.2016.12.032